Top Curr Chem (2011) 304: 91–115
DOI: 10.1007/128_2011_148

Published online: 29 April 2011

Electrorheological Fluid and Its Applications in Microfluidics

Limu Wang, Xiuqing Gong, and Weijia Wen

Abstract Microfluidics is a low-cost technique for fast-diagnosis and microsynthesis. Within a decade it might become the foundation of point-of-care and lab-on-a-chip applications. With microfluidic chips, high-throughput sample screening and information processing are made possible. The picoliter droplet runs in microfluidic chips are ideal miniaturized vessels for microdetection and microsynthesis. Meanwhile, individual manipulation of microdroplets remains a challenge: the shortcomings in automatic, reliable, and scalable methods for logic control prevent further integration of microfluidic applications. The giant electrorheological fluid (GERF), which is a kind of "smart" colloid, has tunable viscosity under the influence of external electric field. Therefore, GERF is introduced as the active controlling medium, with real-time response in on-chip fluid control. This review article introduces the working principles and fabrication methods of different types of electrorheological fluid, and extensively describes the strategies of GERF-assisted microfluidic controlling schemes.

Keywords Electrorheological fluid · Logic control · Microfluidics · Microdroplet

Contents

L. Wang, X. Gong, and W. Wen (✉)
Department of Physics and KAUST-HKUST Micro/Nano-Fluidics Joint Laboratory, The Hong Kong University of Science and Technology, Clear Water Bay, Kowloon, Hong Kong
e-mail: phwen@ust.hk

Abbreviation

AgPDMS	Silver-PDMS composite
CPDMS	Carbon-PDMS composite
CPU	Central processing unit
CTP	Calcium and titanium precipitate
DNA	Deoxyribonucleic acid
ERF	Electrorheological fluid
EWOD	Electrowetting on dielectric
GERF	Giant electrorheological fluid
LOC	Lab-on-a-chip
MCM-41	Mobil composition of matter no. 41
MWNT	Multiwall-nanotube
PANI	Polyaniline
PCR	Polymerase chain reaction
PDMS	Polydimethylsiloxane
PM	Polar-molecule
PMMA	Poly(methyl metharcylate)
POC	Point of care
PPY	Polypyrrole
PS	Polystyrene
SBA-15	Santa Barbara amorphous no.15

1 Introduction

During the last decade, microfluidics emerged as a successfully revitalized, "slimmer" version of fluidics.[1, 2] Through microfluidics, new ground in point-of-care (POC) [3] and lab-on-chip (LOC) [4–6] applications has been carved out. Picoliter droplet runs in microfluidic channels are perfectly suitable for micro-synthesis, drug screening, and chemical tracing; droplets in their discrete nature, moreover, lend themselves analogously to the binary 0/1 coding system, implying, thus, an arithmetic application for microfluidics. Here an interesting question arises: can droplets and bubbles think? [7] What besides the binary logic operations could it provide?

Droplets, in any case, extend the concept of "information" from the binary world characterized by 0/1 to "information as a real entity," such as a DNA sequence and its chemical composition. As Marshall McLuhan famously announced: "The medium is the message". With microfluidic chips, high-throughput sample screening and information processing are made possible, and thousands of individual droplet "message carriers" can be individually dispensed [8]. As a result, high-density microfluidic control unions [9] are required. Despite the off-chip macroscaled solenoid arrays controlled by peripheral equipments, on-chip control components have spurred interest and attracted enormous attention owing to their scalability and cascadability. Among the proposed on-chip control schemes, the electrowetting-on-dielectric (EWOD) system [10, 11] is famous for its fine "digital" control of droplets, yet its predefined round-trip control, reflecting its electronic rather than fluidic nature, diminishes its flexibility. Likewise, individual manipulation of microdroplets remains a challenge: the shortcomings in automatic, reliable, and scalable methods for logic control prevent further integration of microfluidic applications [12]. By employing giant electrorheological fluid (GERF) [13], researchers have realized a series of fully chip-embedded soft-valves and have made strides in fluidic-based automatic droplet control systems.

Electrorheological fluid (ERF), composed of dielectric particles suspended in insulating oil, is a type of smart material that can be utilized as a two-phase system: fluid phase or solid phase. The viscosity of ERF can vary by a few orders of magnitude under the application of an external electric field. If the field is sufficiently strong, ERF can "solidify" into an anisotropic solid boasting a yield stress befitting its strength. The change in rheological characteristics usually is accomplished within 10 ms and is reversible. Hence, ERF has utility as an electrical–mechanical interface [14–16] for potential active-control clutch, damper, and valve applications [17–19], and is denoted "smart".

In this review article, we look at current topics in electrorheological (ER) material design and effect enhancement, including dispersed particles and the dispersing phase, and explore their applications in microfluidic devices for precise manipulation of fluids and droplets.

2 Electrorheological Fluid

The ER phenomenon was first discovered by Winslow in the 1940s; appropriately enough, the "smart" property of this material was initially named "the Winslow effect" [20]. Key experiments since then have established that certain kinds of particles suspended in insulating oils tend to form a fibrous structure in the direction of an applied electric field. Those particles found to be responsive to the electric field usually contain semiconductive solids of high dielectric constants. Early ERF were mostly hydrous, with cellulose, corn starch, silica gel, or zeolite as the dispersed particles [21–23]. The problems with hydrous ERF include weak yield stress under shearing, high corrosion, narrow working temperature ranges, low

suspensibility, and low stability. By the 1980s, renewed experimental and theoretical interests advanced understanding of both the ER mechanism and the fabrication of novel materials with enhanced ER effects [24, 25]. Anhydrous ERF, which is to say, ERF without water or polar solvent in the dispersing phase, has become mainstream and boasts higher yield stress, an increased working temperature, improved stability, and lower zero-field viscosity, and other advantages. Considerable efforts have gone into the preparation of new and various particle suspensions with an eye to improving the ER yield stress. These suspensions include semiconducting organic polymers, inorganic solids with high dielectric constants, and organic–inorganic hybrid material. Particles of differing shape, surface morphology, and dispersing phase also have been closely scrutinized, specifically to increase local surface polarizations.

2.1 Inorganic ER Particles

According to well-known theoretical models, inorganic solids with high dielectric constant have a strong electroresponsive fibrous structure. Typical examples include TiO_2, calcium, strontium or barium titanate precipitates [26], zeolite or clay-type minerals, and polar-molecule-dominated ERFs (PM-ERFs) [27].

TiO_2 is among the most intriguing and well-studied ER materials [24, 28]. Given its high dielectric constant, it has been presumed to be a potential ER-active substrate; however, due to a low active intrinsic structure, it shows only very weak ER activity. Yin et al. doped TiO_2 with Cr ions to improve its ER activity, thereby increasing the defect and charge states and improving the local interfacial polarization effect; they found that the effective yield stress of a typical Cr-doped TiO_2 suspension at 3 kV/mm is 18 times higher that of a pure TiO_2 suspension [29, 30]. Also, assuming that a larger surface area and active interface would further enhance ER activity [31], they employed a block-copolymer-templated sol–gel method to obtain mesoporous TiO_2 of a different porosity. The effective yield stress of their mesoporous, Cr-doped TiO_2 ER suspension was three times higher than that of nonporous Cr-doped TiO_2 ERF, seven times higher than that of mesoporous pure TiO_2 ER suspension, and 20 times higher than that of nonporous pure TiO_2 ER suspension. Moreover, the ER effect of the mesoporous Cr-doped TiO_2 was found to be dependent on the surface area or porosity, and indeed, a high surface area or porosity sample was subsequently demonstrated to have a higher ER activity. Recently, Yin et al. modified the surface morphology of mesoporous Cr-doped TiO_2 to form sea-urchin-like TiO_2, which further improved ER performance. The hierarchical Cr-doped titania (TiO_2) particles consisted of high-density rutile Cr-doped titania nanorods of 20–30 nm diameter assembled radially on the surfaces of the particles. The specific surface area of the particles was close to 65 m^2/g, which was 13 times higher than that of smooth Cr-doped TiO_2 particles, the crystal structure and composition of which, significantly, were similar to those of the hierarchical ones. Their yield stress was approximately twice as high as that

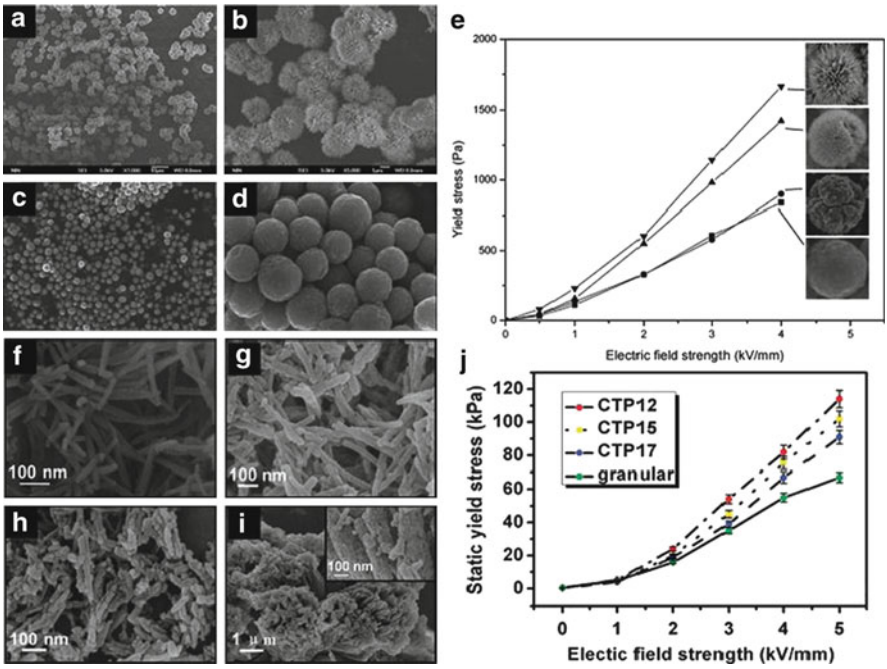

Fig. 1 (**a**, **b**) SEM images of sea-urchin-like hierarchical Cr-doped titania (TiO_2) particles, and (**c**, **d**) smooth Cr-doped TiO_2 particles. (**e**) Yield stress as function of electric field for ERFs of Cr-doped TiO_2 particles and differing surface morphology (*filled square* smooth Cr-doped TiO_2; *filled circle* surface-coarsened Cr-doped TiO_2 without sea-urchin-like nanostructure; *filled triangle* hierarchical Cr-doped TiO_2 with less well-developed sea-urchin-like nanostructure; *filled inverted triangle* hierarchical Cr-doped TiO_2) [32]. (**f–i**) 1D Ca–Ti–O-type nanorods of differing aspect ratio. (**j**) Yield stress as function of electric field for ERFs with CTP nanorods of differing aspect ratio (*dashed lines*) and with a granular CTP suspension (*solid line*) [26]

of the smooth Cr-doped TiO_2 suspension, 3.5 times as high as that of the hierarchical pure TiO_2 suspension, and 13 times as high as that of the smooth pure TiO_2 suspension (Fig. 1) [32].

Since the discovery of the giant ER (GER) effect of Ba–Ti–O-type nanoparticles (Fig. 2) [13, 33, 34], Ca–Ti–O- or Sr–Ti–O-type composites have been exploited for use as ER particles. These particles offer good wetting ability with silicon oil, and their ER effect surpasses the highest reported yield stress for conventional ERFs. To increase the suspension stability, Li et al. used carbon nanotubes to connect Ba–Ti–O particles together in a network structure. Carbon nanotubes prohibit the aggregation and sedimentation of particles, doubling the suspending time without deteriorating the GER effect [35]. Cheng et al. [26], using the co-precipitation method, synthesized one-dimensional (1D) nanorods of calcium and titanium precipitates (CTPs) for a high ER effect. The main components of CTP have been demonstrated to be polycrystalline $CaC_2O_4{\cdot}H_2O$, $TiOC_2O_4(H_2O)_2$, and

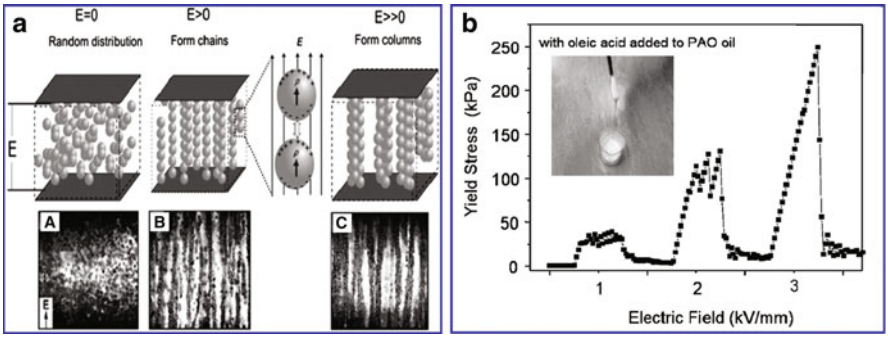

Fig. 2 Working principle of GERF. (**a**) GERF stays in liquid state when no electric field (*E*) is applied, begins to form chains under a moderate field of 500 V/mm, and then grows into columns as electric field increases. (**b**) Yield stress of hydrocarbon oil-based GERF with oleic acid additive, as function of applied electric field [33]

$TiO(OH)_2$. These rod-like particles have highly uniform widths and tunable lengths. Although a high aspect ratio of CTP particles was designed for a high static yield stress, experiment indicates that the effective static yield stress is a function of the electric field, and a moderate aspect ratio of CTP particles provides the highest effective yield stress. The effective static yield stress is defined as the static yield stress at electric field minuses the yield stress at zero electric field, and aspect ratio will also improve the yield stress at zero electric field. Through experiment, it was found that the yield stress of rod-like particles was 3.8 times that of a granular CTP suspension.

Besides TiO_2- and Ba–Ti–O-type materials, mesoporous molecular sieves and clay-type ionic crystalline materials also show admirable ER effects. Taking laponite-type ERFs as an example [36], a minimum electric field of 0.6 kV/mm can trigger laponite polarization and induce chain formation. Governed by the dielectric constant and the external electric field, laponite's rheology is similar to that of spherical-particle-based ER systems. Although the highest static yield stress obtained is lower than 1 kPa under an electric field, the rheology shows Newtonian-like behavior with relatively low shearing stress under a zero electric field.

Shen et al. [27] developed PM-ERFs as an effective means to enhance the ER effect of both TiO_2- and Ba–Ti–O-type materials. Their method adds urea (dipole moment = 4.56 D) or C=O and O–H polar molecules (2.3–2.7 D and 1.51 D) to TiO_2, and adds C=O and O–H polar molecules to Ca–Ti–O and Sr–Ti–O nanoparticles, during their formation. The results showed that the yield stress of the PM-ERFs was greatly enhanced over that of the conventional ERFs. This effect of polar molecules can be verified by heating the particles at high temperature (500–800°C) and removing the absorbed polar groups (confirmed by IR and differential scanning calorimeter measurement), which leads to diminished ER yield stress comparable to that of the traditional dielectric ERFs. Shen et al. also derived a new ERF yield

stress measurement method that roughens the surfaces of electrodes, preventing ERF from sliding under an applied electric field.

2.2 Inorganic–Polymer Hybrid ER Particles

The application of inorganic particles in ERF preparation accrues profitable advantages, including a high dielectric constant, size and shape variability, an accessible interfacial area, and versatility in surface modification. However, the relatively high particle density and low interfacial polarization (when suspending in dispersing fluid) bring about the instability of suspension and low yield stress, which inhibit the practical applications of inorganic ER particles. Hybrid ER particles, such as clay-type particles intercalated by semi-conductive polymers, carbon nanotube hybrid polymers, and metal-doped polymers, embody the organic–inorganic synergistic effect. A variety of polymers, including polystyrene (PS), poly(methyl metharcylate) (PMMA), polyaniline (PANI) and its derivatives, polypyrrole (PPY), and styrene-acrylonitrile, have been hybridized with inorganic materials such as carbon nanotubes, kaolinite, montmorillonite, laponite, mesoporous molecular sieves, and others [37].

Conducting polymers such as PANI- or PPY-intercalated clay-type minerals are another type of ER particle material. Kim et al. synthesized PPY-intercalated montmorillonite nanocomposites through inverted emulsion pathway polymerization, and characterized its ER effect under an electric field [38]. The nanocomposites showed not only a typical ER behavior under electric fields but also the existence of a critical electrical field when the yield stress was plotted as a function of the electric field.

Conducting polymers also can be utilized to form core–shell structures with high dielectric constant particles. Fang et al. used PANI to encapsulate barium titanate via in situ oxidative polymerization. They examined the influence of the fraction of $BaTiO_3$ particles on the ER behavior, and found that the PANI/ $BaTiO_3$ composites-based ERFs exhibit a better ER effect than does pure PANI, which result might be due to the unique ferroelectric properties as well as the high dielectric constant of $BaTiO_3$ nanoparticles.

Cho et al. reported ERFs with conducting PANI and a silica-based mesoporous molecular sieve (MCM-41). The PANI was confined in the channels of the mesoporous MCM-41, partially filling them. It induced enhanced dipole moments in the longitude direction, thereby increasing the ER effect relative to pure MCM-41 [39]. The same results were found for PANI-inserted particles of the mesoporous molecular sieve SBA-15 [40].

Recently, Jin et al. developed carbon-nanotube-absorbed polymeric microspheres and studied their potential application in ERF. Nanotubes were incorporated into the surface of PS and PMMA microspheres. Later, Park et al. investigated the enhanced ER effect of multiwall-nanotubes (MWNTs) on the insulating PMMA [41].

2.3 Conducting-Polymer-Based ER Particles

Semi-conducting polymers with the π-conjugated electron system have a fine electron-donating property but a low ionic potential, and thus can potentially be used as ER materials. These polymers include PANI, PPY, polythiophene, poly (phenylenediamine) and poly(*p*-phenylene), their derivatives, and copolymers. Among these polymers, PANI and its derivatives have been the most commonly reported, owing to their ease of preparation via chemical oxidation polymerization of aniline. PANI can be utilized also as an encapsulating or encapsulated material in the formation of core–shell structures. PANI has various derivatives and thus can be grafted onto inorganic or other organic materials to adjust particle conductivity or density. The core–shell PMMA/PANI microspheres employed as dispersed materials in ERFs represent an example [42].

2.4 Dispersing Phase

ERFs are a type of smart material composed of dielectric particles suspended in insulating oil, and can be utilized as a two-phase system. The flow characteristics of this system depend on both the properties of the dispersed particles and the oil (Fig. 3). The chain length of the oil and the functional groups in the chain can influence the interfacial adhesion strength between the two phases and, consequently, the viscoelastic properties. Such an effect can favor the agglomeration of particles into large clusters by interparticle electrostatic and van der Waals forces. To investigate the oil effect, oils with the same functional groups but different viscosities, and oils with same viscosity but different functional groups, have been studied and the results indicate effectively enhanced yield stresses. The choice of hydroxyl-terminated silicon oil of 25 cSt viscosity resulted in the highest yield stress, 300 kPa [43].

2.5 Future Research Directions

In order to synthesize effective nanosized ER particles, current experimental devices and processes should be modified. This involves controlling the reaction time and solvent temperature, as well as other conditions during the chemical synthesis. It is also crucial to prepare nanoparticles with various dehydration methods under suitable conditions. For example, for the synthesis of inorganic GER particles, researchers have found that pure $BaTiO_3$ nanoparticles do not form a promising ER suspension, even though such particles possess a very high dielectric constant; however, surface modification of such ceramic particles can dramatically improve the ER yield stress. Although water can also greatly enhance the ER yield stress, it suffers from an inherent drawback in that water can evaporate. Therefore, the ER effect is intensely associated with the water molecule concentration, leading

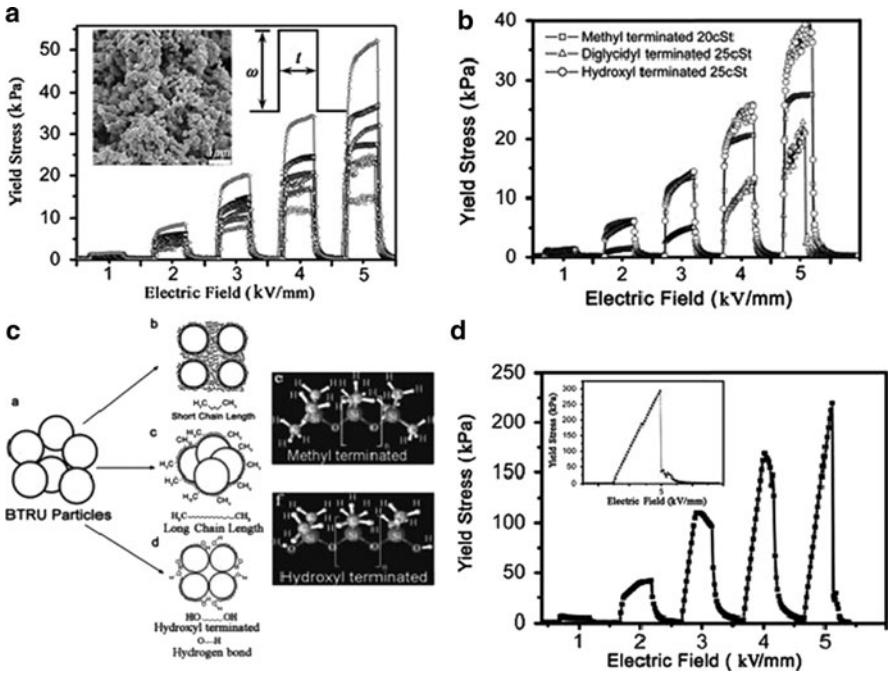

Fig. 3 (**a**) ER effects of seven GERFs constituted of different silicone oils. *Inset*: SEM photograph of the as-prepared BTRU (urea-coated barium titanyl oxalate) particles of around 100 nm diameter. (**b**) Yield stresses measured as function of applied electric field of GERFs constituted of hydroxyl-, methyl-, and diglycidyl-group-terminated silicone oils. (**c**) ERF structures with methyl-terminated silicone oil and hydroxyl-terminated silicone oil. (**d**) Yield stress variation of GERF constituted of hydroxyl-group-terminated silicone oil, measured as function of applied electric field. The concentration is 0.25. The *inset* shows the limiting yield stress value of 300 kPa obtained by direct application of a 5 kV/mm electric field [43]

to unstable and sometimes non-repeatable experimental results. Therefore, the role of water in the ER effect needs to be further explored, and optimization of coating processes to obtain a uniform surface coating layer is also necessary. In addition, the ER effect might also be increased by employing various surfactants with different molecular dipole moments.

It is also found that the liquid phase is crucial in obtaining a good ER suspension and intensive ER effect. The role of silicone oils and other nonconductive liquids should be examined from both experimental and theoretical aspects.

3 ERF-Based Precise Microfluidic Control System

Of all the microfluidic issues, microvalve and droplet logic are among the most basic and crucial areas of research for both one-step fluid actuation and multistep precise fluid control [44–47]. Researchers have never stopped pursuing

an effective, simply structured and easy-to-fabricate microvalve; from the first thin membrane valve proposed by Unger et al. [9] to hydrogel valves [48, 49], heat-control valves [50], and screw-pneumatic valves [51–53], this effort has retained its significance through the decades. The first-generation polydimethylsiloxane (PDMS)-based microfluidic valves comprised two cross-channels separated by a thin PDMS membrane; whereby air pressure coming from the lower channel deflects the thin membrane, which then closes the upper channel and blocks the flow in the upper channel [9]. This membrane-separated cross-channel design has been proved effective, and its principle is still operative to date [54]. Nonetheless, the design is subject to flaws resulting from the laxly effective response of air (a compressible medium), and the unstable pressure brought about by air leakage through the micropores of PDMS. Integratable and digitally addressable microfluidic valves with fast response are rare in microanalysis systems.

GERF (discovered by Wen et.al.) has a yield stress up to 300 kPa in response to an electric field, which provides an alternative choice of digitally controllable microvalve that can respond within 10 μm [13, 43]. Its solid-like behavior sustains shear in the direction perpendicular to the applied electric field, the shear stress can be enhanced when the applied electric field increases, and its rheological variation is reversible upon removal of the electric field (Fig. 4). These marvelous features qualify GERF as an electric-fluid-mechanical interface for digital fluid control in microfluidics [55, 56].

As shown in Fig. 4, when there is no electric field applied to the GERF in the microfluidic channels, it keeps flowing; but when an electric field is applied, the GERF starts to form columns, effecting high yield stress to balance the pumping pressure, leading to flow blockage if the electric field is sufficiently strong. The channel size in microfluidic systems typically is around 10~100 μm. Rather than the high voltage (typically in kilovolts) required in macroscopic applications, the GERF control voltage in microfluidics is limited to ~200 V, a value both feasible and safe in daily life.

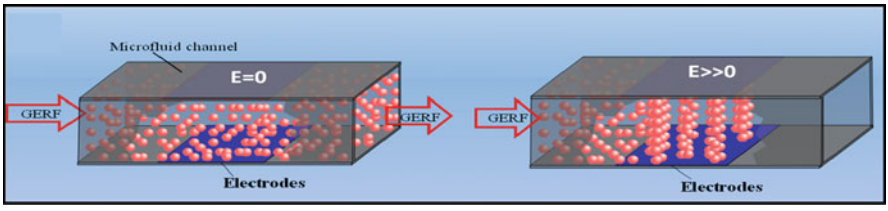

Fig. 4 When no electric field (*E*) is exerted, GERF keeps flowing because it is pumped, and when electric field is applied on GERF by embedded parallel plate electrodes, GERF solidifies. A sufficiently strong electric field will cause a very high GERF yield stress, which will result in the fluid suspending effect

3.1 *Soft Conducting Electrodes for Droplet Detection and ERF On-Chip Control*

PDMS is a silicon-based organic polymer that has been widely used in microfluidic chip fabrication owing to its good elastic property, nontoxicity, biocompatibility, optical transparence, non-inflammability, chemical inertness and conformability, among other attributes [57–61]. Regarding the demand for electrical signal detection and device control in microfluidic chips, integration of conducting structures into bulk PDMS has been a crucial issue. However, PDMS is an inert polymer lacking conductive and magnetic properties. In addition, due to the weak adhesion between PDMS and metal, it is problematic to pattern metallic structures onto its surface or into bulk PDMS for microdevice fabrication.

Recently, Niu et al. developed a method of patterning conductive structures using PDMS-based conducting composites, which are synthesized by uniformly mixing conductive micrometer silver or nanometer carbon particles with PDMS gel [62]; the resultant mixtures, respectively, were denoted AgPDMS and CPDMS. Silver and carbon-black particles, thanks to their desirable wetting characteristics, are easy to mix with PDMS gel. To fabricate the soft conducting composite into PDMS-based chips (Fig. 5a), Niu et al. embedded AgPDMS or CPDMS gel into a photoresist mold (Fig. 5b) on a glass substrate for patterning of conductive composites. After baking, the gel was cured into a solid, and the conducting composite pattern was retained on the substrate by removing the photoresist mold. (The complete fabrication process is described in [62].) The experimental results indicated that two-dimensional (2D) and three-dimensional (3D) conducting microstructures, the dimensions of which can range from tens to hundreds of micrometers, had been

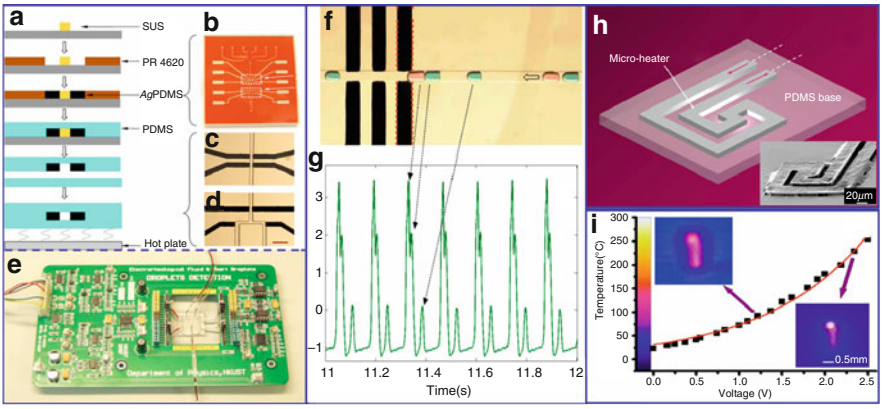

Fig. 5 (**a**–**f**) Method of fabrication of chip-embedded electrode (AgPDMS) [62]. (**e**) On-chip electric detection module. (**f**) Optical image of group of water droplets of different sizes. A small amount of dye was added for labeling [63]. (**g**) Detected signals. (**h**) Microheater fabricated from AgPDMS. (**i**) Response according to applied voltage [64]

successfully constructed and integrated into PDMS bulk material (Fig. 5c, d). The advantage of using PDMS-based conducting composites is the ease of microstructure bonding and embedding into PDMS-based microchips, along with the formation of electric signal connections in a 2D or 3D microstructure, thereby effecting great enhancements in the potential functionalities of microfluidic chips. With the help of AgPDMS or CPDMS, channel-wall-embedded electrodes, leading to highly integrated on-chip droplet detection (Fig. 5e–g) and GERF control, is achievable.

Electrical input, sensing, and detection of microfluidic signals is the alternative to pneumatic and optical methods. A PDMS/glass-based electroporation [65–68] or analytical microsystem [6, 59, 69] requires chip-patterned electrodes. For the purposes of sensing and detecting non-continuous droplet volumes [70, 71], Niu et al. considered that droplet size and distance can vary both spatially and temporally and introduced a capacity detection method for determining droplet size, shape, and composition [63]. By means of a pair of parallel electrodes installed across the microfluidic channel, very small capacitance variations can be detected when a droplet passes through. Thus, due to the electrode's design and feedback electronic circuit (Fig. 5e), real-time and accurate determination of the size, shape, and composition of droplets can be achieved (Fig. 5f, g). Soft conductive patterns can serve not only as electrodes but also as chip-embedded soft microresistors, microheaters (Fig. 5h) [64, 72], and micropressure sensors [72]. Figure 5i shows a plot of the voltage (or current)-dependent temperature control of such a microheater.

3.2 GERF Microvalves

Yoshida et al. [55] and Nakano et al. [73] tested ER effects in SU-8 channels with indium tin oxide electrodes, for self-control of ERF in hard substrates. Niu et al. designed a GERF-based microfluidic valve responsive to external DC signals and was able to develop this concept as a system for microfluidic flow control free of any limitations of flow type [74].

This approach follows Quake's three-layer-architecture microfluidic valve [9]. The design of this soft-lithography-fabricated PDMS-based multilayered four-port microvalve, wherein the controlled fluid and GERF flow along the x- and y-axes, respectively, is schematized in Fig. 6a. The GERF flows in layer 1, replacing the air-valve channel in Quake's design, and parallel CPDMS electrodes are tightly integrated on the two sidewalls of the GERF channel, forming upstream and downstream control valves. The controlled liquid flows in layer 2. As indicated in the intersectional scheme (Fig. 6a), a 35 μm-thick flexible diaphragm lies between the two layers, separating the cross-channels. Figure 6b shows an optical microscopy image of such a microvalve chip. GERF is continuously pushed at a constant pressure into the chip by a syringe pump (Fig. 6c). With an adequate DC electric field applied alternately to two electrode pairs, the pressure in the GER channel between the two valves can be modulated as the two valves are alternately opened

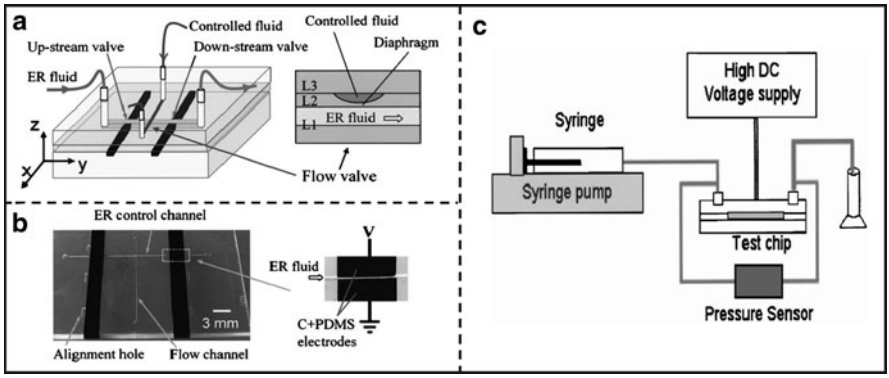

Fig. 6 Design and fabrication of four-port microGER valve. (**a**) Design of four-port valve chip. *Right*: cross-section of the different layers forming the flow valve; *L1* is the GER channel layer, *L2* the controlled flow channel layer, and *L3* the cover layer. (**b**) Optical photograph of fabricated microGER valve chip. *Right*: top-view image of the planner electrodes and the GER channel. (**c**) Experimental setup for microvalve testing [74]

and closed. Such a pressure change within the ER channel will eventually result in the deformation of the flexible diaphragm with a vertical pull-and-push movement. In this way, the liquid flow in flow channel layer 2 is controlled by the pressure changes in the GERF channel.

3.3 Integratable Microfluidic Components Based on GERF Microvalves

This microvalve approach, providing a variable pressure source by means of a chip-embedded microchannel, is a simplified on-chip pressure-control scheme that minimizes the need for peripheral equipment and electronic components, which in any case are difficult to integrate into a microfluidic chip. Apt application of this method can realize many desirable micropump [75], micromixer [76], and micro-platform [77] functions such as those illustrated in Fig. 7.

Given the need to drive fluid inside chips, a micropump is a necessary component of all microfluidic chips, regardless of specific applications. Various types of pumps have been designed and fabricated using different mechanisms, e.g., the air pump is actuated and controlled by gas air-pressure [9, 47], and the piezoelectric transducer actuator pump [78] utilizes electricomechanical energy conversion. The GERF-actuated microfluidic pump (Fig. 7a–c) is digitally programmable, and exhibits good performance at high pumping frequencies along with uniform liquid flow characteristics [75]. In this design, a five-layer structure is embedded inside the PDMS chip, the bottom layer channeling GERF that can affect the flow of the circulating fluid on the top layer via the pull–push movement of the diaphragms

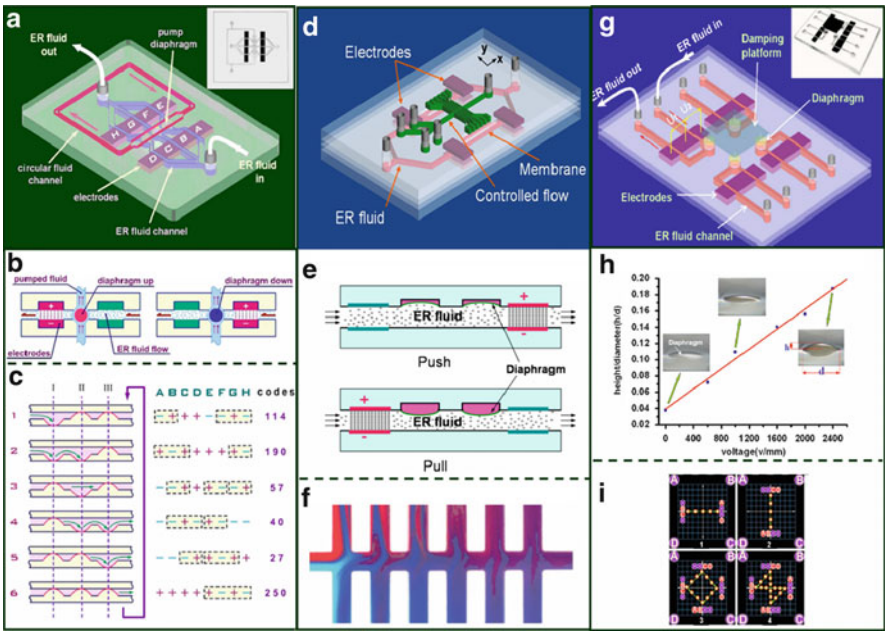

Fig. 7 Microfluidic devices realized by integration of GERF-based microvalve. (**a**–**c**) Micropump by integration of three microvalves [75]. (**a**) Micropump of 3D structure. The GERF-actuated chip controls the fluid circulation in the upper layer. (**b**) Single diaphragm valve via pumped GERF. (**c**) The diaphragm's pumping sequences and their corresponding signals. (**d**–**f**) GERF-actuated mixer design [76]. (**d**) Scheme of mixer construction. (**e**) Side view of push-and-pull GER valve. (**f**) Sinusoidal cross-stream flows in the six pairs of side channels. (**g**–**i**) Microfluidic platform [77]. (**g**) Flexible platform of microfluidic chip. (**h**) Displacement of diaphragms plotted as function of applied electric field across GERF channels. (**i**) Time traces of laser spot reflected from platform are shown on screen with coordinates. Digitally programmed electrical signals to the four ER valves generate the complex leveling modes of the platform to direct the laser spot

between two pairs of electrodes (Fig. 7b). When a control DC signal is applied to the electrode pairs sequentially, pumped flux in the upper layer varies as a function of the intensity and frequency of the electric field. The direction of the fluid flow and the pumped flux also can be controlled through a programmed signal sequence applied to four-electrode pairs (electrodes A–H in Fig. 7b, c).

Mixing two or more streams of fluids is an important issue in various microfluidic devices. The mixing process is not trivial on the microscale, owing to the dominance of the viscous effect and, hence, laminar flow phenomenon. Passive mixers are designed to induce 3D helical fluid motions from patterned structural asymmetries that can fold the streams into highly nested thin slices, so as to facilitate local molecular interdiffusion. Another approach is that of active mixers employing dynamic control to help achieve chaotic mixing. A PDMS-based GERF-driven cross-stream active mixer was reported by Wen et al.

Figure 7d shows a schematic depiction of the active mixer chip design, consisting of a main flow channel and six pairs of orthogonal side channels [76]. Operation of the mixer chip relies on the perturbation of the main *x*-directional channel flow by *y*-directional cross-stream side-channel flows. The side-channel flows are perturbated by pressure changes through thin membranes affected by a GERF microvalve (Fig. 7e). Square-wave electrical voltage signals (0–800 V) are applied between the electrodes to control the microvalve and, in turn, the perturbation, leading to pulsating sinusoidal cross-stream flows in the six pairs of side channels, as shown in Fig. 8f.

The microplatform (sketched in Fig. 7g–i) also works by way of the assistance of microvalves, integrated into the four corners of the chip [77]. The programmed push-and-pull of each microvalve will deform the diaphragms (Fig. 7h) of each valve sequentially, thereby realizing the desired platform function, as shown in Fig. 7i.

3.4 "Smart" Droplet Control by GERF

Despite the successful applications of multilayer-structured valves, researchers have derived a new methodology for on-chip fluid control utilizing the soft/droplet valve. This approach avoids the complexity of the multilayer architecture while maintaining the robustness of GERF-based devices. In these new designs, GERF and target fluid are operated in the same layer (or the same channel), with integrated electrodes on the channel sides. Two protocols have been tested: (1) GERF as carrier flow for target droplets, and (2) GERF droplets as an in-channel soft valve for target fluid or droplets. Thus, new research ground has been broken: GERF-modulated droplet microfluidics, also known as digital microfluidics, in which many digital and logic functions were and have been demonstrated.

As shown in Fig. 8a–f, fluids that are immiscible with GERF can be generated in GER carrier flow [56, 79]. The droplet generation schemes (flow focusing and T junction) are illustrated separately in Fig. 8a, b. As GERF (the carrier flow) is electrically controlled by electrodes placed on the sides of the GER inlet channel and near the fluid junction area, the droplets generated and dispersed (i.e., water, oil, and gas) are no longer uniform in size but can be determined by the controlling electric signal, as shown in Fig. 8c, d. The desired droplet length and separation speed, in other words, can be achieved by electrically controlling the pressure of the carrier flow.

An even more useful functionality of this configuration is active modulation of the relative positions of droplets [56]. Because an electric field can be applied to chip-integrated electrodes, GERF can "solidify" between them and the flow in the relevant channel will be "frozen," as shown in Fig. 8e, f. The relative droplet position can be adjusted in this way. Moreover, as the influence is achieved through medium fluid (GERF), direct application of electric field to target droplets is

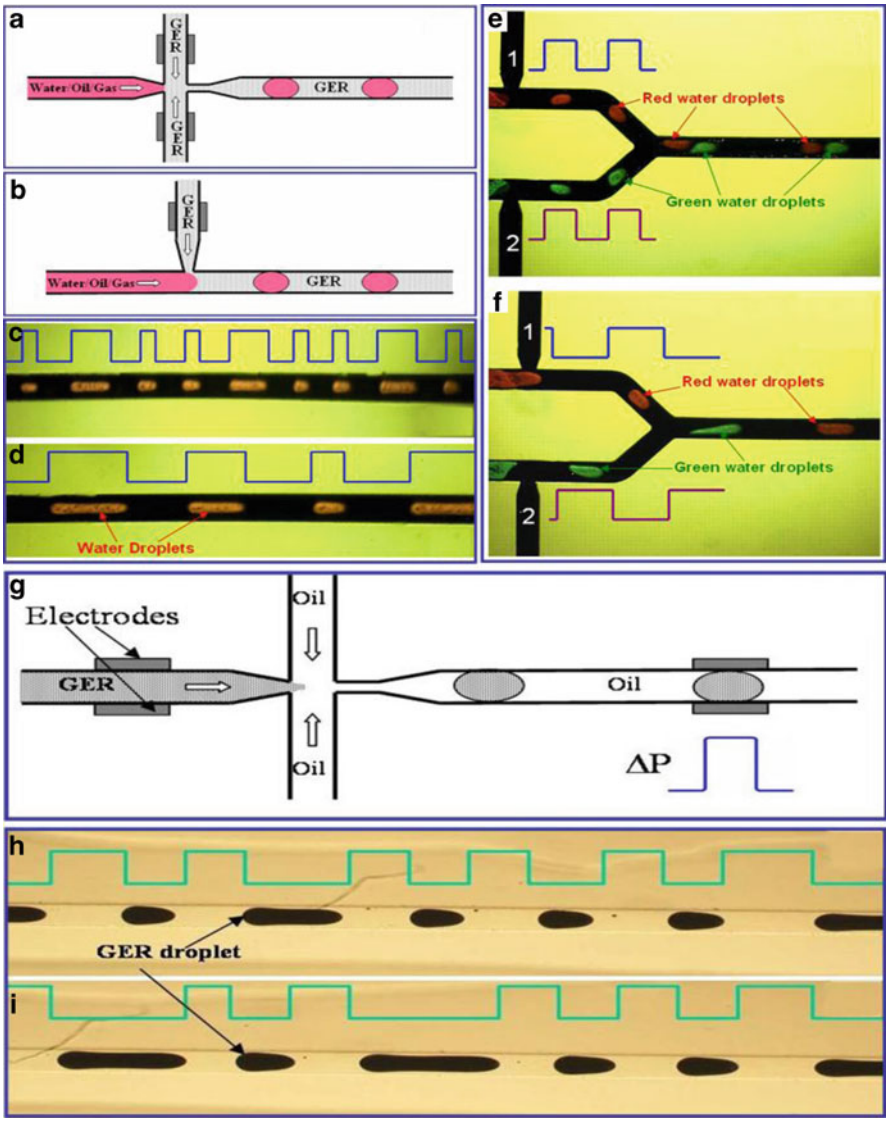

Fig. 8 (**a**–**d**) GERF-assisted droplet generation: (**a**) flow-focusing approach; (**b**) T junction. (**c**, **d**) Electric-field-controlled generation of droplets in a microchannel. *Lines* indicate the electric control signal applied to the electrodes embedded on both sides of the GERF inlets. (**e**, **f**) Digitalized controlled droplets distance [56]. (**g**–**i**) Digital GERF droplet generation: (**g**) schematic view; (**h**,**i**) different droplet patterns under different electric pulse trains [79]

avoided, preventing electrolysis or electrical cell lyses in target droplets. A reverse application of this technique is to put GERF as the dispersed phase, i.e., with fluid as the control, as shown in Fig. 8g. Examples of active digital control of GERF

droplets are shown in Fig. 8h, i. The length of GERF droplets responds exactly to the input electric signals.

These approaches are significant not only for digitalizing in-channel GERF control but also for in-channel soft-valve schemes for more advanced applications, such as droplet display and droplet position modulation. In these applications, GERF (or its droplet) exhibits the capability of an in-channel soft valve, redirecting itself (Fig. 9a, b), guiding other fluid or droplets (Fig. 9c), and even reversing droplet order in channels (Fig. 9d).

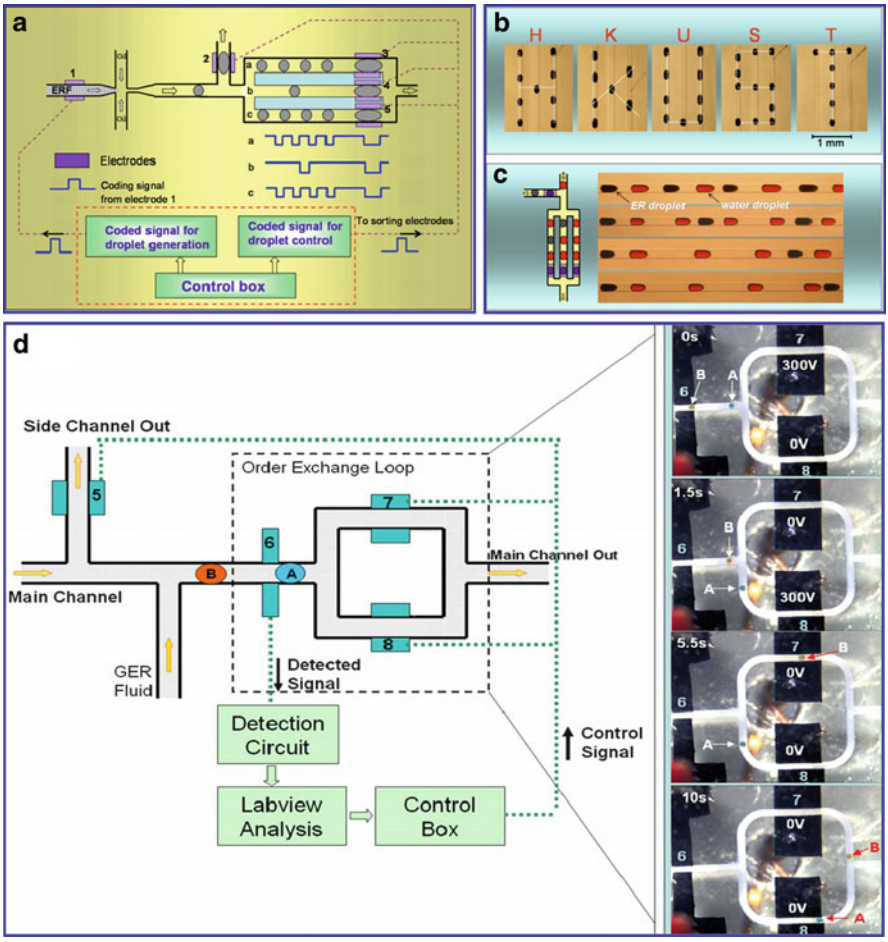

Fig. 9 (**a**–**d**) GERF-assisted smart droplet manipulation. (**a**) Flow chart and control circuit for the generation of a smart droplet display. (**b**) Optical images of the smart droplet display. (**c**) *Left*: chip component showing the orthogonal channels to form the water droplet "packages." *Right*: optical images of the generated packages formed with different numbers of water droplets sandwiched between two smart droplets [79]. (**d**) Flow chart and control circuit for droplet order exchange. *Right*: optical images taken at different times during the exchange process [56]

3.5 *Droplet Logic*

All the latest popular electronic devices, including the iPad, have evolved from the first vacuum tube, i.e., the first electronic logic gate. Now there are more than twenty million logic gates functioning in the CPU of any personal computer. Scientists have endeavored to reinvent this near-legendary component in other systems. Some binary logic functions have been successfully mimicked by fluidic diodes, microelectrochemical logic [80], and conducting-polymer-coated microelectrode arrays [81]. In microfluidic domains, researchers have scrutinized both kinetic fluid regulation [47, 82, 83] and static geographical stream manipulation [84–87] as possible solutions. Simple logic devices such as the AND/OR gate, the static fluid transistor, and the oscillator are some of the achievements. They are limited, however, in that they entail either bulky peripheral equipment for round-trip manipulation, or have complicated 3D microstructures. Moreover, they are confined by the soft-lithographic technique with which they are formed. Because they are designed within pre-shaped architectures for distinct tasks, they have no reprogrammability or cascadability. Another solution is the aforementioned EWOD method, in which every single step of droplet move is well defined, in an electronic approach [10, 11, 88, 89].

Real digital microfluidic devices should resemble computers instead of preset "music boxes". They should simplify control schemes while preserving the delicacy of microdevices, and should be "smart" enough to "think" by themselves [7], indicating that the outputs that should fully depend on inputs in assigned tasks. In microfluidics, researchers have demonstrated this possibility in both the stream regulation method and in bubble/droplet schemes. By introducing the GERF smart colloid, Wen's group was able to invent a new branch of fully automatic droplet logic control: the droplet logic gate. The traditional electric switch controlling the GER ON/OFF phase change is replaced by conductive/high dielectric droplets flowing in a nearby channel, thereby realizing droplet-controlled microfluidic logic (on-chip droplet control) [90]. Fabricated by a standard soft-lithographic process [63], its planar structure is simple and, thus, fully compatible with existing microfluidics. Its chip-embedded electrodes can serve collectively as a data-exchanging interface between fluidic and electronic computer systems, enabling their seamless integration. We can foresee its applications to microfluidic information processors, transacting control, and memory operations on the basis of droplet trains in which nonlinear chemical dynamics, complex neuron communication, or DNA computing is performed. Its operative principle is illustrated in Fig. 10.

Thanks to soft conducting composites, through soft-lithography, microfluidic channels can be planar arranged and electrically connected by AgPDMS. The input of this device, droplets between electrodes as switches, can be modeled as impedance in circuits. That is, alterable impedance in fluidic form can be used to adjust the voltage applied to GERF or as the ON/OFF switch of the GERF phase change. A sufficiently large constant voltage is supplied across the two electrodes to solidify the GERF under the desired conditions. Preferably, the signal fluid is an ionized,

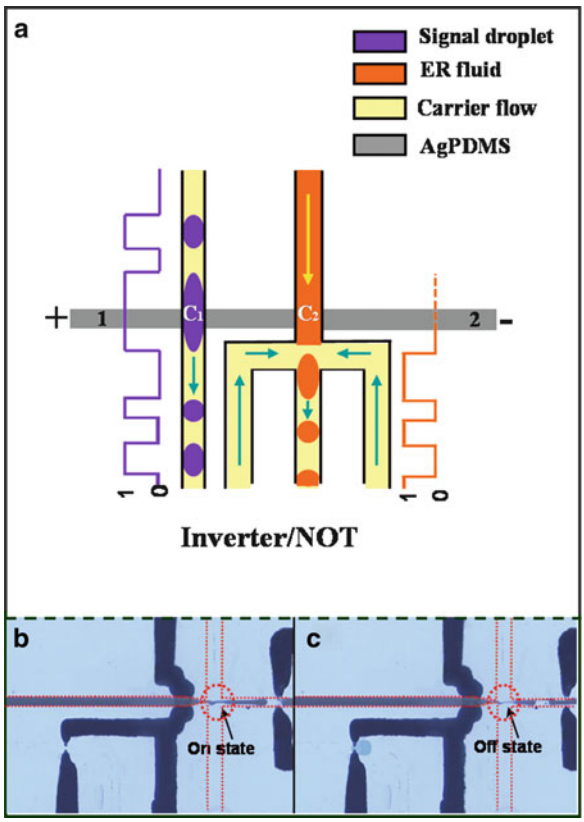

Fig. 10 Basic working principle of logic gate, illustrated by microfluidic inverter. (**a**) Basic working principle. The presence of a signal droplet between the signal electrodes will solidify GERF, whereas the presence of carrier flow will release GERF. (**b**) When the carrier flow is flowing between the signal electrodes, GERF flows continuously. (**c**) When the signal droplet passes by the signal electrodes, GERF solidifies between those electrodes, and is cut into droplets [90]

high-conductivity solution (which can be modeled as a resistor or conductor) or a high-dielectric-constant fluid (which can be modeled as a capacitor), and the carrier flow is an insulating fluid. When the carrier flow presents between the signal electrodes (input 0), the circuit is in an open state, and the GERF continues flowing (defined output: binary 1). When the signal droplet presents between the signal electrodes (input 1), the circuit is in a closed state, and the electric field generated stops the flow of the GERF (defined output: binary 0). When the signal fluid is a dielectric fluid, the fluid in the signal channel can be modeled as a capacitor and denoted as $C_1(x)$, where $x = 0$ if the input is carrier flow or $x = 1$ if the input is signal droplets. The capacitance generated by the GERF is denoted as C_2. In this case, if the applied voltage is V and the voltage share of the GERF is $V_{ER}(x)$, we obtain:

$$V_{ER}(x) = \frac{C_2}{C_1(x) + C_2} V. \tag{1}$$

Further, we can adjust input voltage V to ensure that $V_{ER}(1)$ is larger than the GERF solidification voltage and that $V_{ER}(0)$ is smaller than the crucial value. By

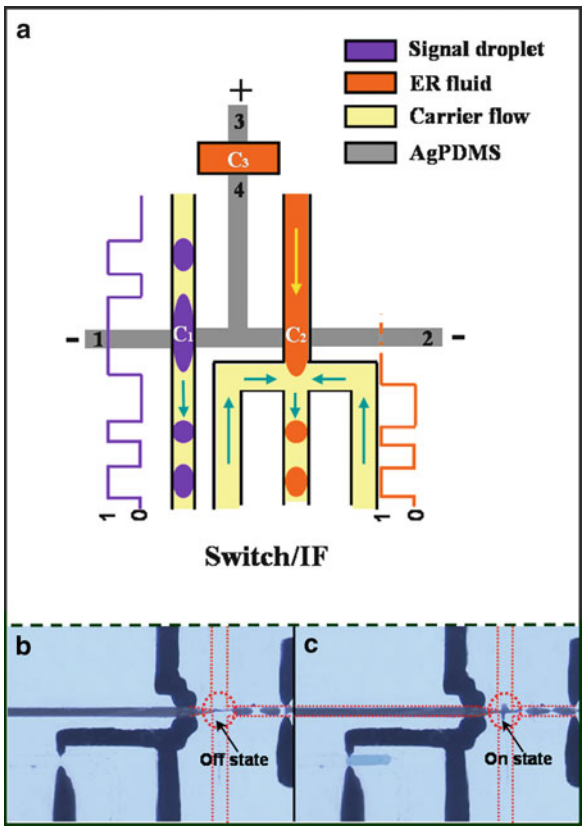

Fig. 11 Working principle of microfluidic switch. (**a**) Microfluidic logic switch is built by adding a capacitor (in the present case, another microfluidic channel filled with steady GERF) to the logic inverter. (**b**) When carrier flow presents between the signal electrodes, GERF solidifies. (**c**) When signal droplets present between the signal electrodes, GERF liquefies and flows out [90]

application of this principle, a fluidic inverter (NOT gate) can be realized. As shown in the experimental results, when there is signal fluid (water droplet) between the signal electrodes, the GERF will stop, and a GER droplet is formed (Fig. 10c); otherwise, the GERF will flow continuously (Fig. 10b).

A fluidic switch is designed according to the principle of a logic inverter, specifically by electrically connecting a capacitor to reverse the logic state of the inverter, as shown in Fig. 11a. The capacitor should have a capacitance comparable to that of the GERF, in order to effectively share voltage with the GERF output channel; when the signal droplet is present between the signal electrodes, the voltage share of the GERF is smaller than the crucial value for its phase change. A simple design methodology is to set the voltage input on electrode 1 to be the electrical conjugation of the voltage input on electrode 2, as shown in Fig. 11a. When the signal droplet is dielectric fluid, we can derive a simplified capacitance model: the input voltage from electrodes 1, 2, 3 is V_1, V_2 and V_3, and the capacitance in the signal channel is $C_1(x)$, where $x = 0$ when the carrier flow is between the signal electrodes and $x = 1$ when the signal droplet passes by the signal electrodes. C_2 is the capacitance of the GERF between the output electrodes, and C_3 is the

capacitance of the added capacitor. $V_{ER}(x)$ is the voltage share of the GERF under a different input situation, the value of $V_{ER}(x)$ being:

$$V_{ER}(x) = \frac{(V_2 - V_3)C_3 + (V_1 - V_2)C_1(x)}{C_3 - C_1(x) - C_2}, \tag{2}$$

where V_1, V_2, and V_3 can be tuned for a desired voltage arrangement, making the GERF solidify when a signal droplet comes by or, conversely, change back to the fluid state when the droplet passes the signal electrodes. To rule out variation of the dielectric constant among different batches of GER powder, we used an additional steady GERF channel (with embedded electrodes) of identical dimensions with GERF output channel to compose an additional fluidic capacitor (shown in Fig. 11a). The case of ionized buffer signal droplets is straightforward to understand, and can be illustrated by our experimental results (see Fig. 11b, c).

The advantage of our microfluidic logic switch and inverter is that two counterpart functions are realized in one single-chip structure. Alternation between the two functions is achieved by selective voltage input, or by connection or disconnection of electrode pads. It is always desirable to have fewer units working to more purposes, for simplicity of logic device architecture and better reprogrammability [91]. Because a logic switch and inverter are the basic units of logic operations, a system comprising these two units can have additional functions simply by rearranging the voltage input, obviating any need for restructuring.

4 Family Tree and Development of GERF-Based Microdevices

By way of conclusion, we have sketched a family tree (Fig. 12) of ERF and the related techniques for realization of microfluidic control in microfluidic chips. Through improvements made to ER effects and the development of soft conducting composites, researchers have been able to integrate those techniques with microfluidics in order to digitalize droplets of nano- to picoliter size and achieve droplet logic, storage, and display modules.

The flexibilities in this family of microfluidic techniques are all functions of the distinctly smart material employed: GERF. This treble-function medium can be compared with an electric current: the fluidic output is the response, the dielectric information is the electric medium, and the control of fluid is the mechanical yield source. Sharing compatible working principles, the demonstrated GERF-actuated microfluidic mixer, storage, display, and droplet phase modulator functionalities are all compatible with each other. Liu et al. demonstrated a highly integrated DNA-amplifying microfluidic chip by employing technology in this family tree [92]. In the near future, simple combinations of IF/NOT microdroplet logics could lead to microfluidic processors, analogs to microelectronic computers. To take it

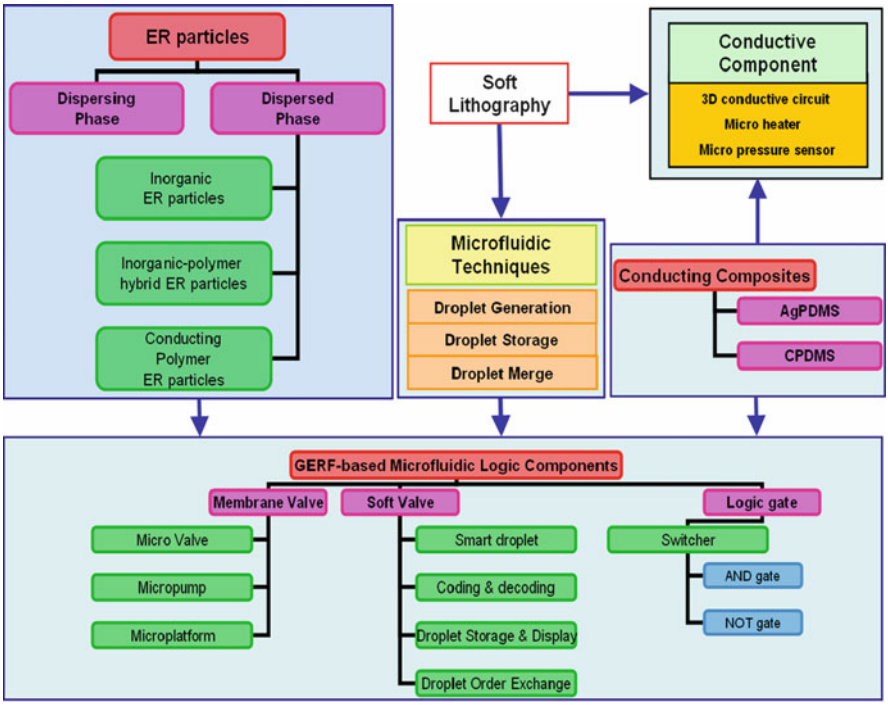

Fig. 12 Family tree of ERF-based microfluidic technologies

one step further, integration of all of the techniques described above might lead to a GERF-based microfluidic computing system. Moreover, the components of this suggested system all have chip-embedded electrodes, which can serve as information interfaces with electronic devices, promising a highly integrated system comprised of a computer and microfluidic processors.

Inevitably, the processing capability of this logic device (GERF response is 10 ms) will be compared with that of computers (electronic processes take nanoseconds). The delay can be meliorated by adjusting the flow speed and flow-focusing geometry, but not eliminated. It needs to be borne in mind that microfluidics and electronics deal with different issues: microfluidics is not expected to become a mainframe computing system but is earmarked for exploratory, LOC research and POC applications (e.g., portable diagnosis kits), areas in which conventional computers have their own intrinsic shortcomings. The future of microfluidics lies not in computing but in multidimensional information processing. Microfluidics in any case retains its inherent promise: an extension of the fluidic information realm beyond "binary 0/1" to the spatial, chromatic, or physiological dimension [69, 71, 88, 93]. Preloaded chemical or biological information can be well preserved in droplet form. Droplet PCR, for example, can easily store and recreate genetic information [94]. Microfluidics provides a unique tool for handling and processing biological, chemical, environmental, genetic, and

chromatic information. Considering the contribution of DNA logic to fuzzy computing [95, 96], which indeed can be elaborated in picoliter droplets, it is really difficult to foresee a bound future of microfluidics if tools like DNA computing are incorporated.

We can imagine a microfluidic processor, performing important control and memory operations on the basis of droplet trains. Nonlinear chemical dynamics, complex neuron communication, or DNA computing might be carried out in every single droplet of this processor, and these droplets could couple together for more complex tasks. Electromagnetic technology extended the human sensory system and enabled us to sense the world through a portable device. Through microfluidic technology, we are extending a part of ourselves (blood, tissue, cell, or DNA) to microchips, and beyond. The GERF-assisted microfluidic technology can combine the extended "human body" and "human sensory system" on a piece of microfluidic chip, in a fully automatic sense. It will be interesting to see the outcomes of such a coupled system.

Acknowledgements This publication is based on work supported by Award No. SA-C0040/UK-C0016, made by King Abdullah University of Science and Technology (KAUST) and Hong Kong RGC grants HKUST 603608.

References

1. McDonald JC, Duffy DC, Anderson JR et al (2000) Electrophoresis 21:27
2. Quake SR, Scherer A (2000) Science 290:1536
3. Dudek MM, Lindahl TL, Killard AJ (2010) Anal Chem 82:2029
4. Srinivasan V, Pamula VK, Fair RB (2004) Lab Chip 4:310
5. Lin BC, Gao Y, Qin JH (2009) J Chin Chem Soc 56:1
6. Malic L, Brassard D, Veres T et al (2010) Lab Chip 10:418
7. Epstein IR (2007) Science 315:775
8. Beer NR, Rose KA, Kennedy IM (2009) Lab Chip 9:841
9. Unger MA, Chou H, Thorsen T et al (2000) Science 288:113
10. Pollack MG, Fair RB, Shenderov AD (2000) Appl Phys Lett 77:1725
11. Fair RB (2007) Microfluid Nanofluid 3:245
12. Su F, Chakrabarty K, Fair RB (2006) IEEE Trans Comput Aided Des Integr Circ Syst 25:211
13. Wen W, Huang X, Yang S et al (2003) Nat Mater 2:727
14. Tao R, Sun JM (1991) Phys Rev Lett 67:398
15. Halsey TC (1992) Science 258:761
16. Ma H, Wen W, Tam WY et al (2003) Adv Phys 52:343
17. Papadopoulos CA (1998) Mechatronics 8:719
18. Choi W, Tuteja A, McKinley GH (2009) Adv Mater 21:2190
19. Hao T (2001) Adv Mater 13:1847
20. Winslow WM (1949) J Appl Phys 20:1137
21. Li Y, Chen Y, Conrad H (1995) ASME 235:29
22. Conrad H, Li Y, Chen Y (1995) J Rheol 39:1041
23. Wu CW, Conrad H (1996) J Phys D 29:3147
24. Lu KQ, Shen R, Wang XZ et al (2005) Int J Mod Phys B 19:1065
25. Lu KQ, Shen R, Wang XZ et al (2006) Chin Phys 15:2476

26. Cheng Y, Wu K, Liu F et al (2010) ACS Appl Mater Interfaces 2:621
27. Shen R, Wang X, Lu Y et al (2009) Adv Mater 21:4631
28. Shen R, Wang XZ, Wen WJ et al (2005) Int J Mod Phys B 19:1104
29. Yin JB, Zhao XP (2004) Chem Mater 16:321
30. Zhao XP, Yin JB (2002) Chem Mater 14:2258
31. Yin JB, Zhao XP (2006) J Phys Chem B 110:12916
32. Yin J, Zhao X, Xiang L et al (2009) Soft Matter 5:4687
33. Shen C, Wen W, Yang S et al (2006) J Appl Phys 99:106104
34. Wen WJ, Huang XX, Sheng P (2004) Appl Phys Lett 85:299
35. Li J, Gong X, Chen S et al (2010) J Appl Phys 107:093507
36. Parmar KPS, Meheust Y, Schjelderupsen B et al (2008) Langmuir 24:1814
37. Yoshimoto S (2005) Macromol Rapid Commun 26:857
38. Kim JW, Liu F, Choi HJ et al (2003) Polymer 44:289
39. Cho MS, Choi HJ, Ahn WS (2004) Langmuir 20:202
40. Cho MS, Choi HJ, Kim KY et al (2002) Macromol Rapid Commun 23:713
41. Park SJ, Cho MS, Lim ST et al (2005) Macromol Rapid Commun 26:1563
42. Cho MS, Cho YH, Choi HJ et al (2003) Langmuir 19:5875
43. Gong X, Wu J, Huang X et al (2008) Nanotechnology 19:165602
44. Zeng S, Li B, Su X et al (2009) Lab Chip 9:1340
45. Hosokawa K, Maeda R (2000) Micromech Microeng 10:415
46. Hosokawa K, Fujii T, Endo I (1999) Anal Chem 71:4781
47. Groisman A, Enzelberger M, Quake SR (2003) Science 300:955
48. Yu Q, Bauer JM, Moore JS et al (2001) Appl Phys Lett 78:2589
49. Beebe DJ, Moore JS, Bauer JM et al (2000) Nature 404:588
50. Pal R, Yang M, Johnson BN et al (2004) Anal Chem 76:3740
51. Elizabeth Hulme S, Shevkoplyas SS, Whitesides GM (2009) Lab Chip 9:79
52. Zheng Y, Dai W, Wu H (2009) Lab Chip 9:469
53. Weibel DB, Kruithof M, Potenta S et al (2005) Anal Chem 77:4726
54. Weibel DB, Siegel AC, Lee A et al (2007) Lab Chip 7:1832
55. Yoshida K, Kikuchi M, Park JH et al (2002) Sens Actuators A Phys 95:227
56. Zhang M, Wu J, Niu X et al (2008) Phys Rev E 78:066305
57. Eddings MA, Johnson MA, Gale BK (2008) J Micromech Microeng 18:067001
58. Leclerc E, Sakai Y, Fujii T (2003) Biomed Microdevices 5:109
59. Moreira NH, Almeida AL, Piazzeta MH et al (2009) Lab Chip 9:115
60. Ng JMK, Gitlin I, Stroock AD et al (2002) Electrophoresis 23:3461
61. Sia SK, Whitesides GM (2003) Electrophoresis 24:3563
62. Niu X, Peng S, Liu L et al (2007) Adv Mater 19:2682
63. Niu X, Zhang M, Peng S et al (2007) Biomicrofluidics 1:044101
64. Liu L, Peng S, Niu X et al (2006) Appl Phys Lett 89:223521
65. Valero A, Post JN, van Nieuwkasteele JW et al (2008) Lab Chip 8:62
66. Fox MB, Esveld DC, Valero A et al (2006) Anal Bio Chem 385:474
67. Khine M, Lau A, Ionescu-Zanetti C et al (2005) Lab Chip 5:38
68. Young H, Boris R (2003) Sens Actuators A Phys 104:205
69. Derveaux S, Stubbe BG, Roelant C et al (2008) Anal Chem 80:85
70. DeMello AJ (2006) Nature 442:394
71. Kutter JP (2000) Trac Trends Anal Chem 19:352
72. Wang L, Zhang M, Yang M et al (2009) Biomicrofluidics 3:034105
73. Nakano M, Katou T, Satou A et al (2002) J Intell Mater Syst Struct 13:503
74. Niu X, Wen W, Lee YK (2005) Appl Phys Lett 87:243501
75. Liu L, Chen X, Niu X et al (2006) Appl Phys Lett 89:083505
76. Niu X, Liu L, Wen W et al (2006) Appl Phys Lett 88:153508
77. Liu L, Niu X, Wen W et al (2006) Appl Phys Lett 88:173505
78. Nguyen NT, Truong TQ (2004) Sens Actuators B 97:137–143

79. Niu X, Zhang M, Wu J et al (2009) Soft Matter 5:576–581
80. Zhan W, Crooks R (2003) J Am Chem Soc 125:9934
81. Wang X, Zhou J, Tam TK et al (2009) Bioelectrochemistry 77:69
82. Thorsen T, Maerkl SJ, Quake SR (2002) Science 298:580
83. Rhee M, Burns MA (2009) Lab Chip 9:3131
84. Weaver JA, Melin J, Stark D et al (2010) Nat Phys 6:218
85. Prakash M, Gershenfeld N (2007) Science 315:832
86. Mosadegh B, Kuo C, Tung Y et al (2010) Nat Phys 6:433
87. Cheow LF, Yobas L, Kwong D (2007) Appl Phys Lett 90:054107
88. Srinivasan V, Pamula VK, Fair RB (2004) Anal Chim Acta 507:145
89. Pamula VK, Srinivasan V, Chakrapani H et al (2005) Proc IEEE Int Conf Micro Electro Mech Syst MEMS :722
90. Wang L, Zhang M, Li J et al (2010) Lab Chip 10:2869
91. Rhee M, Burns MA (2008) Lab Chip 8:1365
92. Liu L, Cao W, Wu J et al (2008) Biomicrofluidics 2:034103
93. Wheeler AR, Throndset WR, Whelan RJ et al (2003) Anal Chem 75:3581
94. Beer NR, Hindson BJ, Wheeler EK et al (2007) Anal Chem 79:8471
95. Adleman LM (1994) Science 266:1021
96. Benenson Y, Gil B, Ben-Dor U, Adar R et al (2004) Nature 429:423